A FINITE DIFFERENCE MODEL FOR ARTICULATED SLIDE-STRING SIMULATION

Abhiram Bhanuprakash, Maarten van Walstijn and Paul Stapleton*

Sonic Arts Research Centre
School of Electronics, Electrical Engineering and Computer Science
Queen's University Belfast
Belfast, UK
{a.bhanuprakash,m.vanwalstijn,p.stapleton}@qub.ac.uk

ABSTRACT

Slide-string instruments allow continuous control of pitch by articulation with a slide object whose position of contact with the string is time-varying. This paper presents a method for simulation of such articulation. Taking into account sensing and musical practice considerations, an appropriate physical model configuration is determined, which is then formulated in numerical form using a finite difference approach. The model simulates the attachment and detachment phases of slide articulation which generally involve rattling, while finger damping is modelled in a more phenomenological manner as a regionally induced time-varying damping. A stability bound for the numerical model is provided via energy analysis, which also reveals the driving power contributions of the separate articulatory sources. The approach is exemplified with simulations of slide articulatory gestures that involve glissando, vibrato and finger damping.

1. INTRODUCTION

Sliding on a string is a special form of articulation used by musicians primarily to produce a continuously varying pitch. It features in various musical practices around the world, including Blues, Country, Hawaiian music as well as in the playing of fretless Indian string instruments such as the chitra veena and mohan veena.

Slide-string instrumentalists use an object made of glass, metal, plastic, wood or horn (in the case of the chitra veena) to press against the string and slide over it. Figure 1 illustrates the typical spatial layout involved in such articulation, featuring a string drawn taut between a nut and a bridge. The string is plucked closer to the bridge. In addition to sliding on the string, players often use their fingers to damp the string and suppress unwanted sounds. Typically, the finger(s) or palm of the left hand are used to damp the non-speaking length of the string, whereas the plucking finger (or plectrum) on the right hand is also used to suppress the transient caused by the attachment of the slide to the string. The associated finger damping regions are shown as grey shaded areas in Figure 1.

During slide articulation, the position of contact between the slide object and the string varies over time. The slide interaction

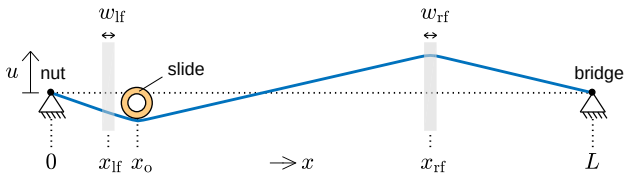

Figure 1: *Spatial layout of the slide-string articulation, with finger force regions indicated by grey shaded areas.*

dynamics is determined partly by linear properties of the musician-controlled slide-hand system, such as its resonance and damping. In addition to this, the dynamics also features non-linear behaviour during phases where the slide attaches to or detaches from the string. It has long been understood that capturing such non-linear and time-varying phenomena in discrete-time models is key in developing physics-based sound synthesis algorithms that can form the basis of realistic-sounding virtual-acoustic instruments [1, 2, 3, 4].

Only a handful of previous studies have focused specifically on slide-string synthesis [5, 6, 7]. In [5], the authors present a digital waveguide (DWG)-based model of a slide guitar that includes the emulation of the frictional sliding noise. In this model, the length of a DWG is varied over time, using a fractional delay filter to produce a smoothly varying pitch. To account for the non-physical energy variations that are caused by on-line string length adjustment, the authors use a method of energy compensation [8, 9]. In [6] the need to address such issues is avoided by introducing a time-varying scattering junction at the slide-string contact point based on a balanced perturbation method proposed in [10], and in addition methods are proposed for modelling slide-string interaction in the horizontal and longitudinal transversal polarisations.

More recently, finite difference (FD) methods have been successfully used to simulate complex non-linear interactions in string instruments [3, 11, 12, 13, 14, 15]. In these works, based on the FD formulation, rigorous, energy-based stability analysis has been established. In this paper, FD methods are employed to discretise a string model that allows slide articulation in ways that closely emulate the established kinaesthetics of slide-string instruments.

A natural way of obtaining the required control signals for such articulation is through sensing the player's actions. As such, it is important to consider sensing criteria in conjunction with the usual physical modelling criteria (accuracy, efficiency, computational robustness), while also taking into account the wider contexts of relevant musician practices and performance cultures. A

* This work was supported by the European Union's Horizon 2020 research and innovation programme under the Marie Skłodowska-Curie grant agreement No 812719.

range of online videos of musicians (see, e.g. on Blues guitar [1] and the mohan veena [2]) were studied to better understand skilful slide articulation, with particular focus on hand and finger movements. In addition, the second author experimented with slide articulation on an acoustic guitar and in doing so gained an embodied understanding of the process, which was further informed by the third author, who is a practising musician. Building on this knowledge, we were able to make informed decisions on the specific sensing input requirements for our model, which in turn dictate the model's control variables. The following strategic modelling choices were made in the design process in order to best meet such holistic considerations:

- The vertical motion of the slide is modelled as driven by string contact and hand compliance forces, both of which are expected to shape and influence the sonic character of slide phrasing.
- The configuration of the slide-hand system features vertical hand position and horizontal slide position as its control variables, which aligns well with the envisaged requirements and options for sensing of the relevant control signals.
- Slide-string collisions are modelled using a unity exponent nonlinear power law in a single variable, which allows modelling rattling involving near-rigid collisions using an explicit update form without the need for over-sampling.
- Finger-string interaction is modelled in a distributed fashion to ensure sufficient finger damping can be achieved.
- To avoid multiple nonlinearities, finger-string attachment and detachment are not modelled as collisions, but in a simplified manner with a damping that fades in/out in proportion to the external finger force. Further, finger-string restoring force is simplified to an external force.
- In order to facilitate efficient local updates at the interaction points, an explicit FD string scheme is used.

2. ARTICULATED SLIDE-STRING MODEL

2.1. Physical modelling configuration

One of the primary choices in defining an articulated slide-string physical model is around how to configure the slide-string interaction. Figure 2 presents four possible configurations for the general case of object-string interaction in the vertical polarisation, in the order of increasing detail captured. Configuration (a), which simply imposes a unilateral barrier at position y_o, is similar to the bridge-string interaction model employed in [16]. This contrasts with (b), which can be regarded as a lossless version of the finger-string interaction model proposed in [3], in that (b) features an object with a finite mass and requires a force rather than a position representing the control variable.

In this paper configuration (c) is chosen to model slide-string interaction, based on the following criteria:
(i) *Where possible, sensing must be performed in a way that does not affect the player's performatory actions.* Position can be sensed using a contactless modality, for example, with optical techniques, and thus has no foreseeable effect on the playing. Conversely, sensing the force of the hand on the slide object may need contact-based measurement modalities, which might call for additional

[1] https://www.youtube.com/watch?v=L7P6S75oleM
[2] https://www.youtube.com/watch?v=x1lUO5WgQ6I

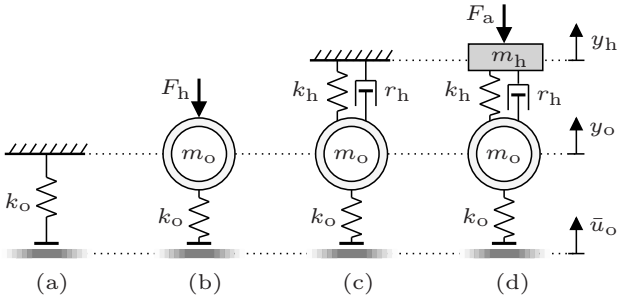

Figure 2: *Four possible physical modelling configurations of object-string interaction in the order of increasing detail captured.*

circuit connections between the slide object and the data acquisition system, which then restricts the freedom of the player's hand movements. Thus, configurations (a) and (c) are better suited from sensing and performance perspectives.
(ii) Position sensing accuracy is critical at specific points. For example, a collision transient would be produced slightly before or after the moment of real-world contact with a controller unless the position sensing is calibrated at the contact point; it is envisaged that such a spatial misalignment could significantly undermine the musician's articulatory accuracy. Therefore, *it is imperative to avoid position estimation drift*, as this is difficult if not impossible to calibrate for. Sensing a force (as done in (b) and (d)) and using a position-based modelling strategy essentially involves performing double integration, which is known to be prone to drift and noise, e.g. inertial position sensing using an accelerometer [17]. Hence, this criterion also suggests (a) and (c) are better choices.
(iii) *The configuration should capture the dynamic characteristics that are of sonic and articulatory importance.* It is envisaged that this includes the resonance and damping of the hand that controls the slide position, which are modelled in configuration (c).

Indeed, we can go one level up to (d) that models the arm force acting on the hand. However, the physical validity of modelling the hand as a passive mass controlled by the arm is debatable, as the hand in reality is controlled by its own muscles. In other words, the value and validity of the added complexity of configuration (d) and any similar attempts to model the hand and arm as vibrating objects is questionable.

2.2. Equations of motion

As shown by Figure 1 and Figure 2 (c), the slide object is modelled here as a finite mass m_o located at position $(x_\mathrm{o}, y_\mathrm{o})$ on a string defined over $\mathcal{S} = [0, L]$. The hand position $(x_\mathrm{o}, y_\mathrm{h})$ is a control input. Let us denote the stiffness and damping co-efficients of the slide-hand connection as k_h and r_h, respectively, as shown in Figure 2 (c).

With this framework, the equation of motion of the slide-string system in Figure 1 with string stiffness, damping, finger-string contact forces and collision with the slide object can be written as:

$$\rho A \frac{\partial^2 u}{\partial t^2} = \mathfrak{C}[u] + \mathcal{F}_\mathrm{rf} + \mathcal{F}_\mathrm{lf} + \mathcal{F}_\mathrm{o}, \tag{1}$$

where the operator $\mathfrak{C}[u]$ is defined as:

$$\mathfrak{C}[u] = T\frac{\partial^2 u}{\partial x^2} - EI\frac{\partial^4 u}{\partial x^4} - 2\rho A\sigma_0 \frac{\partial u}{\partial t} + 2\rho A\sigma_2 \frac{\partial^3 u}{\partial x^2 \partial t}, \tag{2}$$

and where $u = u(x,t)$ is the string transversal displacement, ρ, A, T, E, I, σ_0 and σ_2 are the mass density, cross-sectional area, tension, Young's modulus, moment of inertia, frequency-independent and frequency-dependent damping constants of the string, respectively. The motion of the slide is governed by:

$$m_\mathrm{o}\frac{\partial^2 y_\mathrm{o}}{\partial t^2} = -F_\mathrm{o} - k_\mathrm{h} q_\mathrm{h} - r_\mathrm{h}\frac{\partial q_\mathrm{h}}{\partial t}, \tag{3}$$

where F_o is the contact force, and $q_\mathrm{h} = (y_\mathrm{o} - y_\mathrm{h})$.

2.3. Slide-string contact

The contact force F_o is modelled to have a spatial distribution ψ_o. Let us define:

$$q_\mathrm{o} = \widetilde{u}_\mathrm{o} - y_\mathrm{o}, \tag{4}$$

where

$$\widetilde{u}_\mathrm{o}(t) = \int_0^L \psi_\mathrm{o}(x,t)\, u(x,t) dx \tag{5}$$

is the local string displacement average at x_o, with $\widetilde{u}_\mathrm{o} = \widetilde{u}_\mathrm{o}(t)$ and $y_\mathrm{o} = y_\mathrm{o}(t)$. In line with previous work [14, 11, 3, 16], the contact force density is defined as $\mathcal{F}_\mathrm{o}(x,t) = \psi_\mathrm{o}(x,t)F_\mathrm{o}(t)$, where in the current study, the distribution function and contact force are defined as:

$$\psi_\mathrm{o}(x,t) = \delta(x - x_\mathrm{o}(t)), \tag{6}$$

$$F_\mathrm{o} = -k_\mathrm{o}\lfloor q_\mathrm{o} \rfloor = -\frac{\partial V_o}{\partial q_o}, \tag{7}$$

where $F_\mathrm{o} = F_\mathrm{o}(t)$, $\lfloor u \rfloor = h(u)u$, and where $h(.)$ is the Heaviside function. This expression amounts to applying a Hertzian contact law with unity exponent and stiffness constant k_o. The associated contact potential $V_\mathrm{o} = V_\mathrm{o}(t)$ is:

$$V_\mathrm{o} = \frac{1}{2} k_\mathrm{o} \lfloor q_\mathrm{o} \rfloor^2. \tag{8}$$

2.4. Finger-string contact

Here we model the finger force simply as the sum of an external force and a damping force in the same region. Unlike the string's inherent frequency-independent damping, this damping is induced by the external force and only exists locally in the region of finger-string contact. Thus, the model accounts for pushing and damping forces from the left-hand finger, and pluck and damping forces from the right-hand finger. We denote the left and right-hand finger external forces as F_lf and F_rf, their spatial distributions as ψ_lf and ψ_rf, which are centred around x_lf and x_rf and have widths w_lf and w_rf, respectively, as shown in the grey shaded areas in Figure 1. Further, we denote left and right-hand finger induced damping coefficients as r_lf and r_rf, respectively. The left and right-hand finger force densities, $\mathcal{F}_\mathrm{lf}$ and $\mathcal{F}_\mathrm{rf}$ respectively, can be defined as:

$$\mathcal{F}_\phi(x,t) = \psi_\phi(x,t)F_\phi(t) - \overline{r}_\phi(x,t)\frac{\partial u}{\partial t}, \quad \phi = \mathrm{lf}, \mathrm{rf}, \tag{9}$$

where $\overline{r}_\phi(x,t) = r_\phi(t)\psi_\phi(x,t)$, and where

$$\psi_\phi(x,t) = \begin{cases} \frac{1}{w_\phi} & : |x - x_\phi| \leq \frac{w_\phi}{2} \\ 0 & : \text{otherwise.} \end{cases} \tag{10}$$

The induced damping coefficient is varied in proportion to the finger external force magnitude as:

$$r_\phi(t) = \alpha_\mathrm{f}|F_\phi(t)|, \quad \phi = \mathrm{lf}, \mathrm{rf}, \tag{11}$$

where $\alpha_\mathrm{f} \geq 0$, represents a proportionality constant. This choice is motivated by the observation that the player exerts more external force to damp more. To simplify the left-hand finger position control, the abscissa of the left-hand finger is assumed here to be at a fixed distance x'_lf from x_o, i.e, $x_\mathrm{lf} = x_\mathrm{o} - x'_\mathrm{lf}$.

2.5. Boundary Conditions

We assume simply supported boundaries:

$$u(0,t) = u(L,t) = 0, \quad \frac{\partial^2 u}{\partial x^2}(0,t) = \frac{\partial^2 u}{\partial x^2}(L,t) = 0. \tag{12}$$

2.6. Output signal

As a suitable output signal, we can take the force exerted by the string on the bridge [18]:

$$F_\mathrm{b}(t) = \left(-T\frac{\partial u}{\partial x} + EI\frac{\partial^3 u}{\partial x^3}\right)\Big|_{x=L}. \tag{13}$$

2.7. Energy analysis

Let us define an inner product of two functions f_1 and f_2 and the associated norm as:

$$\langle f_1, f_2 \rangle_\mathcal{S} = \int_0^L f_1 f_2\, dx, \qquad \|f_1\|_\mathcal{S}^2 = \langle f_1, f_1 \rangle_\mathcal{S}. \tag{14}$$

Taking the inner product of (1) with $\frac{\partial u}{\partial t}$ over the domain $\mathcal{S}$, and multiplying (3) by $\frac{\partial y_\mathrm{o}}{\partial t}$, a power-balance equation for the coupled slide-string system can be derived as:

$$\frac{dH}{dt} = (P_\mathrm{rf} + P_\mathrm{lf} + P_\mathrm{o}) - (Q_\mathrm{s} + Q_\mathrm{rf} + Q_\mathrm{lf} + Q_\mathrm{o}), \tag{15}$$

where $H = H_\mathrm{s} + H_\mathrm{o}$ is the Hamiltonian of the slide-string system, with H_s and H_o representing the Hamiltonians of the string (without slide contact) and slide (including string contact), respectively:

$$H_\mathrm{s} = \frac{\rho A}{2}\left\|\tfrac{\partial u}{\partial t}\right\|_\mathcal{S}^2 + \frac{T}{2}\left\|\tfrac{\partial u}{\partial x}\right\|_\mathcal{S}^2 + \frac{EI}{2}\left\|\tfrac{\partial^2 u}{\partial x^2}\right\|_\mathcal{S}^2, \tag{16}$$

$$H_\mathrm{o} = \frac{1}{2}m_\mathrm{o}\left(\frac{dy_\mathrm{o}}{dt}\right)^2 + \frac{1}{2}k_\mathrm{h}q_\mathrm{h}^2 + V_\mathrm{o}. \tag{17}$$

The system driving powers are given by:

$$P_\phi = F_\phi \int_0^L \psi_\phi \frac{\partial u}{\partial t}\, dx, \quad \phi = \mathrm{rf}, \mathrm{lf}, \tag{18}$$

$$P_\mathrm{o} = \left(r_\mathrm{h}\frac{dy_\mathrm{o}}{dt} - k_\mathrm{h}q_\mathrm{h}\right)\frac{dy_\mathrm{h}}{dt} - F_\mathrm{o}\frac{d\widetilde{u}_\mathrm{o}}{dt}, \tag{19}$$

where

$$\frac{d\widetilde{u}_\mathrm{o}}{dt} = \frac{dx_\mathrm{o}}{dt}\frac{\partial u}{\partial x}\Big|_{x=x_\mathrm{o}} + \frac{\partial u}{\partial t}\Big|_{x=x_\mathrm{o}} \tag{20}$$

The dissipation terms are:

$$Q_\mathrm{o} = r_\mathrm{h}\left(\frac{dy_\mathrm{o}}{dt}\right)^2, \quad Q_\mathrm{s} = 2\rho A\left(\sigma_0\left\|\tfrac{\partial u}{\partial t}\right\|_\mathcal{S}^2 + \sigma_2\left\|\tfrac{\partial^2 u}{\partial t \partial x}\right\|_\mathcal{S}^2\right), \tag{21}$$

$$Q_\phi = \int_0^L \overline{r}_\phi \left(\frac{\partial u}{\partial t}\right)^2 dx, \quad \phi = \mathrm{rf}, \mathrm{lf}. \tag{22}$$

Observe from equations (19) and (20) that P_o has a component due to the vertical motion of the hand ($\frac{dy_\mathrm{h}}{dt}$ term), a component due to the horizontal slide motion ($\frac{dx_\mathrm{o}}{dt}$ term), and a component due to the string velocity at x_o ($\frac{\partial u}{\partial t}\big|_{x=x_\mathrm{o}}$ term).

3. NUMERICAL FORMULATION

Let us denote spatial and temporal steps respectively as Δ_x and $\Delta_t = \frac{1}{f_s}$, where f_s is the sampling frequency. A continuous function $\theta(x,t)$ at location $x = m\Delta_x$ and at time $t = n\Delta_t$ is represented in the discrete domain by a grid function $\theta_m^n = \theta(m\Delta_x, n\Delta_t)$, $m \in \underline{\mathcal{M}}$, where $\underline{\mathcal{M}} = \{0, 1, ..., M\}$, and where $M = floor(\frac{L}{\Delta_x})$. Further, we denote the number of internal nodes on the string as $N = M - 1$.

3.1. Difference and sum operators

First-order difference operators in time and space are defined as follows:

$$\delta_t u_m^n = u_m^{n+\frac{1}{2}} - u_m^{n-\frac{1}{2}} \approx \Delta_t \frac{\partial u}{\partial t}\Big|_{x=m\Delta_x,\, t=n\Delta_t}, \tag{23}$$

$$\delta_x u_m^n = u_{m+\frac{1}{2}}^n - u_{m-\frac{1}{2}}^n \approx \Delta_x \frac{\partial u}{\partial x}\Big|_{x=m\Delta_x,\, t=n\Delta_t}. \tag{24}$$

From equations (23) and (24) we can derive second-order difference operators as:

$$\delta_t^2 u_m^n = u_m^{n+1} - 2u_m^n + u_m^{n-1} \approx \Delta_t^2 \frac{\partial^2 u}{\partial t^2}\Big|_{x=m\Delta_x,\, t=n\Delta_t}, \tag{25}$$

$$\delta_x^2 u_m^n = u_{m+1}^n - 2u_m^n + u_{m-1}^n \approx \Delta_x^2 \frac{\partial^2 u}{\partial x^2}\Big|_{x=m\Delta_x,\, t=n\Delta_t}. \tag{26}$$

We also define a backward and a three-point first-order time difference operator as:

$$\delta_{t-} u_m^n = u_m^n - u_m^{n-1} \approx \Delta_t \frac{\partial u}{\partial t}\Big|_{x=m\Delta_x,\, t=n\Delta_t}, \tag{27}$$

$$\delta_{t\cdot} u_m^n = u_m^{n+1} - u_m^{n-1} \approx 2\Delta_t \frac{\partial u}{\partial t}\Big|_{x=m\Delta_x,\, t=n\Delta_t}. \tag{28}$$

Sum operators can be defined as:

$$\mu_t u_m^n = u_m^{n+\frac{1}{2}} + u_m^{n-\frac{1}{2}} \approx 2u\Big|_{x=m\Delta_x,\, t=n\Delta_t}, \tag{29}$$

$$\mu_{t\cdot} u_m^n = u_m^{n+1} + u_m^{n-1} \approx 2u\Big|_{x=m\Delta_x,\, t=n\Delta_t}. \tag{30}$$

3.2. Discrete distributions

The distributions ψ_ϕ can be numerically represented as:

$$\overline{g}_{\phi,m}^n = \frac{1}{\Delta_x}\int_0^L \psi_\phi(x, n\Delta_t)\nu_m(x)dx, \quad \phi = \mathrm{rf}, \mathrm{lf}, \mathrm{o}. \tag{31}$$

Here, $\nu_m(x)$ denotes a *catchment function* for the m^{th} node, which is chosen to be a triangular function spread over two neighbouring nodes on either side, and defined as:

$$\nu_m(x) = \begin{cases} \frac{x}{\Delta_x} + (1-m) & : (m-1)\Delta_x \le x < m\Delta_x \\ -\frac{x}{\Delta_x} + (1+m) & : m\Delta_x \le x \le (m+1)\Delta_x \\ 0 & : \text{otherwise.} \end{cases} \tag{32}$$

3.3. Finite difference scheme

Using the notation developed in sections (3.1) and (3.2), an FD scheme for the system in equation (1) can be written as:

$$\delta_t^2 u_m^n = \mathfrak{D}'[u_m^n] + \xi\overline{g}_{\mathrm{rf},m}^n F_\mathrm{rf}^n + \xi\overline{g}_{\mathrm{lf},m}^n F_\mathrm{lf}^n - \alpha(\overline{r}_{\mathrm{rf},m}^n + \overline{r}_{\mathrm{lf},m}^n)\delta_{t\cdot} u_m^n + \xi\overline{g}_{\mathrm{o},m}^n F_\mathrm{o}^n, \tag{33}$$

where $\mathfrak{D}'[u_m^n] = \lambda^2\delta_x^2 u_m^n - \beta^2\delta_x^4 u_m^n - \gamma_0\delta_{t\cdot} u_m^n + \gamma_2\delta_{t-}\delta_x^2 u_m^n$ and with

$$\lambda = \sqrt{\frac{T}{\rho A}}\frac{\Delta_t}{\Delta_x}, \quad \beta = \sqrt{\frac{EI}{\rho A}}\frac{\Delta_t}{\Delta_x^2}, \quad \gamma_0 = \sigma_0\Delta t, \quad \gamma_2 = \frac{2\sigma_2\Delta t}{\Delta_x^2}, \quad \xi = \frac{\Delta_t^2}{\rho A}, \quad \alpha = \frac{\Delta_t}{2\rho A}, \tag{34}$$

$$\overline{r}_{\phi,m}^n = \overline{g}_{\phi,m}^n r_\phi^n, \quad \phi = \mathrm{lf}, \mathrm{rf}. \tag{35}$$

Here δ_{t-} is chosen to discretise the time derivative in the frequency-dependent damping term in order to make the scheme explicit, as in [11]. From (7), F_o^n can be numerically written as:

$$F_\mathrm{o}^n = -\frac{\delta_{t\cdot} V_\mathrm{o}^n}{\delta_{t\cdot} q_\mathrm{o}^n}. \tag{36}$$

The discrete counterpart of (3) governing the motion of m_o is:

$$m_\mathrm{o}\frac{\delta_t^2 y_\mathrm{o}^n}{\Delta_t^2} = -F_\mathrm{o}^n - k_\mathrm{h}\frac{\mu_{t\cdot}(y_\mathrm{o}^n - y_\mathrm{h}^n)}{2} - r_\mathrm{h}\frac{\delta_{t\cdot}(y_\mathrm{o}^n - y_\mathrm{h}^n)}{2\Delta_t}. \tag{37}$$

From (12), the numerical boundary conditions can be written as:

$$u_0^n = u_M^n = 0; \quad \delta_x^2 u_0^n = \delta_x^2 u_0^n = 0. \tag{38}$$

Discretising (13) using (38) and defining $b_\lambda = \frac{T}{2\Delta_x}$, $b_\beta = \frac{EI}{2\Delta_x^3}$, the numerical bridge force can be derived as:

$$F_\mathrm{b}^n = 2b_\lambda u_{M-1}^n + 2b_\beta(2u_{M-1}^n - u_{M-2}^n). \tag{39}$$

3.4. Numerical energy analysis

As a discrete-domain counterpart of (14), a discrete inner product and the associated norm are defined as:

$$\langle f_{1,m}^n, f_{2,m}^n\rangle_\mathcal{X} = \sum_{m\in\mathcal{X}} f_{1,m}^n f_{2,m}^n \Delta_x, \quad \left\|f_{1,m}^n\right\|_\mathcal{X}^2 = \langle f_{1,m}^n, f_{1,m}^n\rangle_\mathcal{X}. \tag{40}$$

Also, a set lacking the last node is defined as $\underline{\mathcal{M}} = \{0, 1, ..., N\}$ and a set containing only the inner nodes is defined as $\mathcal{M} = \{1, 2, ..., N\}$. Now, taking the inner product of (33) with $\frac{\delta_{t\cdot} u_m^n}{2\Delta_t}$ over the domain $\underline{\mathcal{M}}$, and multiplying (37) by $\frac{\delta_{t\cdot} y_\mathrm{o}^n}{2\Delta_t}$, a power-balance equation for the coupled slide-string system can be derived as:

$$\frac{\delta_t H^n}{\Delta_t} = (P_\mathrm{rf}^n + P_\mathrm{lf}^n + P_\mathrm{o}^n) - (Q_\mathrm{s}^n + Q_\mathrm{rf}^n + Q_\mathrm{lf}^n + Q_\mathrm{o}^n), \tag{41}$$

where $H^{n+\frac{1}{2}} = H_\mathrm{s}^{n+\frac{1}{2}} + H_\mathrm{o}^{n+\frac{1}{2}}$, with $H_\mathrm{s}^{n+\frac{1}{2}}$ and $H_\mathrm{o}^{n+\frac{1}{2}}$ being:

$$H_\mathrm{s}^{n+\frac{1}{2}} = \frac{\rho A}{2}\left\|\frac{\delta_t u_m^{n+\frac{1}{2}}}{\Delta_t}\right\|_{\underline{\mathcal{M}}}^2 + \frac{T}{2}\left\langle\frac{\delta_x u_{m+\frac{1}{2}}^{n+1}}{\Delta_x}, \frac{\delta_x u_{m+\frac{1}{2}}^n}{\Delta_x}\right\rangle_{\underline{\mathcal{M}}} + \frac{EI}{2}\left\langle\frac{\delta_x^2 u_m^{n+1}}{\Delta_x^2}, \frac{\delta_x^2 u_m^n}{\Delta_x^2}\right\rangle_\mathcal{M} - \frac{\sigma_2\rho A\Delta_t}{2}\left\|\frac{\delta_t\delta_x u^{n+\frac{1}{2}}_{m+\frac{1}{2}}}{\Delta_t\Delta_x}\right\|_{\underline{\mathcal{M}}}^2, \tag{42}$$

$$H_{\mathrm{o}}^{n+\frac{1}{2}} = \frac{1}{2} m_{\mathrm{o}} \left(\frac{\delta_t y_{\mathrm{o}}^{n+\frac{1}{2}}}{\Delta_t} \right)^2 + \frac{1}{2} k_{\mathrm{h}} \left(\frac{\mu_t q_{\mathrm{h}}^{n+\frac{1}{2}}}{2} \right)^2 + \frac{\mu_t V_{\mathrm{o}}^{n+\frac{1}{2}}}{2}. \tag{43}$$

In equation (41),

$$P_\phi^n = F_\phi^n \left\langle \overline{g}_{\phi,m}^n, \frac{\delta_t . u_m^n}{2\Delta_t} \right\rangle_{\underline{\mathcal{M}}}, \quad \phi = \mathrm{rf}, \mathrm{lf}, \tag{44}$$

$$P_{\mathrm{o}}^n = \left(r_{\mathrm{h}} \frac{\delta_t . y_{\mathrm{o}}^n}{2\Delta_t} - k_{\mathrm{h}} \frac{\mu_t . q_{\mathrm{h}}^n}{2} \right) \frac{\delta_t . y_{\mathrm{h}}^n}{2\Delta_t} - F_{\mathrm{o}}^n \frac{\delta_t . \widetilde{u}_{\mathrm{o}}^n}{2\Delta_t}, \tag{45}$$

$$Q_{\mathrm{s}}^n = 2\rho A \sigma_0 \left\| \frac{\delta_t . u_m^n}{2\Delta_t} \right\|_{\underline{\mathcal{M}}}^2 + 2\sigma_2 \rho A \left\| \frac{\delta_t . \delta_x u_{m+\frac{1}{2}}^n}{2\Delta_t \Delta_x} \right\|_{\underline{\mathcal{M}}}^2, \tag{46}$$

$$Q_\phi^n = \left\langle \overline{r}_{\phi,m}^n, \left(\frac{\delta_t . u_m^n}{2\Delta_t} \right)^2 \right\rangle_{\underline{\mathcal{M}}}, \quad \phi = \mathrm{rf}, \mathrm{lf}, \tag{47}$$

$$Q_{\mathrm{o}}^n = r_{\mathrm{h}} \left(\frac{\delta_t . y_{\mathrm{o}}^n}{2\Delta_t} \right)^2. \tag{48}$$

Note that the discrete power-balance mirrors its continuous counterpart except for the frequency-dependent loss term, which is a tradeoff we need to make for an explicit scheme (see Section 3.5 and [11, 1]). The stability criterion for the scheme can be derived as a condition on the non-negativity of H^n [11, 1]. Writing $\mathfrak{T} = \frac{T\Delta_t^2}{\rho A} + 4\sigma_2 \Delta_t$, we have:

$$\Delta_x \geq \sqrt{\frac{1}{2} \left(\mathfrak{T} + \sqrt{\mathfrak{T}^2 + \frac{16 E I \Delta_t^2}{\rho A}} \right)}. \tag{49}$$

3.5. Vector-matrix update form of spatial subsystems

To solve efficiently, at each time step, the system in (33) is partitioned in space into subsystems by defining [3]:

$$\mathcal{M} = \mathcal{M}_{\mathrm{nc}}^n \cup \mathcal{M}_{\mathrm{rf}}^n \cup \mathcal{M}_{\mathrm{lf}}^n \cup \mathcal{M}_{\mathrm{o}}^n, \tag{50}$$

where

$$\mathcal{M}_\phi^n = \{ m \in \mathcal{M} : \overline{g}_{\phi,m}^n \neq 0 \}, \quad \phi = \mathrm{rf}, \mathrm{lf}, \mathrm{o}, \tag{51}$$

$$\mathcal{M}_{\mathrm{nc}}^n = \{ m \in \mathcal{M} : \overline{g}_{\mathrm{rf},m}^n = \overline{g}_{\mathrm{lf},m}^n = \overline{g}_{\mathrm{o},m}^n = 0 \}. \tag{52}$$

Also, let us denote the cardinality of $\mathcal{M}_\phi^n$ as $|\mathcal{M}_\phi^n|, \phi = \mathrm{rf}, \mathrm{lf}, \mathrm{o}, \mathrm{nc}$. For the system in (33), we define the displacement vector:

$$\mathbf{u}^n = \left[u_1^n, \ldots u_N^n \right]^T, \tag{53}$$

where ^{T} represents matrix transpose. The second and fourth spatial derivative matrices are defined, respectively, as:

$$\mathbf{D}_2 = \begin{bmatrix} -2 & 1 & & 0 \\ 1 & \ddots & \ddots & \\ & \ddots & \ddots & 1 \\ 0 & & 1 & -2 \end{bmatrix}_{N \times N}, \tag{54}$$

$$\mathbf{D}_4 = \mathbf{D}_2^2. \tag{55}$$

[3] nc, rf, lf and o stand for non-contact, right-hand finger, left-hand finger and slide object, respectively.

Let us denote $\mathbf{u}_\phi^n$ to be the reduced displacement vectors, i.e, the vectors having entries $u_m^n, m \in \mathcal{M}_\phi^n, \phi = \mathrm{rf}, \mathrm{lf}, \mathrm{o}, \mathrm{nc}$. Similarly, let $\mathbf{g}_\phi^n$ represent the reduced distribution vectors having entries $\overline{g}_{\phi,m}^n, m \in \mathcal{M}_\phi^n, \phi = \mathrm{rf}, \mathrm{lf}, \mathrm{o}$. Further, let $\mathbf{P}_{m,*}$ denote the submatrix of a matrix $\mathbf{P}$, containing m^{th} rows of $\mathbf{P}$. Using this notation, we define the second and fourth spatial derivative matrices (of dimensions $|\mathcal{M}_\phi^n| \times N$) as:

$$\mathbf{D}_{2,\phi}^n = \mathbf{D}_{2_{m,*}}, m \in \mathcal{M}_\phi^n, \phi = \mathrm{rf}, \mathrm{lf}, \mathrm{o}, \mathrm{nc}, \tag{56}$$

$$\mathbf{D}_{4,\phi}^n = \mathbf{D}_{4_{m,*}}, m \in \mathcal{M}_\phi^n, \phi = \mathrm{rf}, \mathrm{lf}, \mathrm{o}, \mathrm{nc}. \tag{57}$$

In addition, we define:

$$\mathbf{R}_\phi^n = |\mathcal{M}_\phi^n| \times |\mathcal{M}_\phi^n| \text{ diagonal matrix with diagonal entries } \overline{r}_{\phi,m}^n, m \in \mathcal{M}_\phi^n, \phi = \mathrm{rf}, \mathrm{lf}. \tag{58}$$

With this notation, the numerical counterpart of equation (5) can be written as:

$$\widetilde{u}_{\mathrm{o}}^n = \left(\mathbf{g}_{\mathrm{o}}^n \right)^T \mathbf{u}_{\mathrm{o}}^n \Delta_x. \tag{59}$$

We can write the vector-matrix update form of each subsystem as:

$$\mathbf{u}_{\mathrm{nc}}^{n+1} = \mathfrak{L}_{\mathrm{nc}}, \tag{60}$$

$$\mathbf{A}_\phi \mathbf{u}_\phi^{n+1} = \mathfrak{L}_\phi, \phi = \mathrm{rf}, \mathrm{lf}, \tag{61}$$

$$\mathbf{u}_{\mathrm{o}}^{n+1} = \mathfrak{L}_{\mathrm{o}} + E_{\mathrm{o}}' F_{\mathrm{o}}^n \mathbf{g}_{\mathrm{o}}^n, \tag{62}$$

where the linear term $\mathfrak{L}_\phi$ is defined as:

$$\mathfrak{L}_\phi = \begin{cases} B_\phi \mathbf{u}_\phi^n + C_\phi \mathbf{u}_\phi^{n-1} + \mathbf{B}_\phi' \mathbf{u}^n + \mathbf{C}_\phi' \mathbf{u}^{n-1}, & \phi = \mathrm{nc}, \mathrm{o} \\ B_\phi \mathbf{u}_\phi^n + \mathbf{C}_\phi \mathbf{u}_\phi^{n-1} + \mathbf{B}_\phi' \mathbf{u}^n + \mathbf{C}_\phi' \mathbf{u}^{n-1} & \\ \qquad + \xi F_\phi^n \mathbf{g}_\phi^n, & \phi = \mathrm{rf}, \mathrm{lf}. \end{cases} \tag{63}$$

The equations for the matrices and constants involved in (60) - (63) are given in the appendix. As the scheme is explicit, (60) and (61) can be solved explicitly. Equation (62) is the only non-trivial update equation, since it involves the unknown non-linear force F_o^n. To solve for F_o^n, we define:

$$s_{\mathrm{o}} = q_{\mathrm{o}}^{n+1} - q_{\mathrm{o}}^{n-1}. \tag{64}$$

Using (36), (8) and (64), F_{o}^n can also be written as:

$$F_{\mathrm{o}}^n = -\frac{k_{\mathrm{o}}}{2} \frac{\lfloor s_o + q_o^{n-1} \rfloor^2 - \lfloor q_o^{n-1} \rfloor^2}{s_o}. \tag{65}$$

To turn the subsystem (62) into a scalar equation, we pre-multiply both sides with $\left(\mathbf{g}_{\mathrm{o}}^{(n+1)} \right)^T \Delta_x$. Doing this and using (59), (64) and the gridded version of (4), we have:

$$s_{\mathrm{o}} + q_{\mathrm{o}}^{n-1} + y_{\mathrm{o}}^{n+1} = \left(\mathbf{g}_{\mathrm{o}}^{(n+1)} \right)^T \Delta_x (\mathfrak{L}_{\mathrm{o}} + E_{\mathrm{o}}' F_{\mathrm{o}}^n \mathbf{g}_{\mathrm{o}}^n). \tag{66}$$

Note that y_{o}^{n+1} is also unknown. Using (37), we have:

$$y_{\mathrm{o}}^{n+1} = \mathcal{B}' y_{\mathrm{o}}^n + \mathcal{C}' y_{\mathrm{o}}^{n-1} + \mathcal{D}' + \mathcal{E}' F_{\mathrm{o}}^n, \tag{67}$$

whose update matrices and constants are given in the appendix. Substituting (67) in (66), we get:

$$s_o + \mathcal{B} + \mathcal{C} \frac{\lfloor s_o + q_o^{n-1} \rfloor^2 - \lfloor q_o^{n-1} \rfloor^2}{s_o} = 0, \tag{68}$$

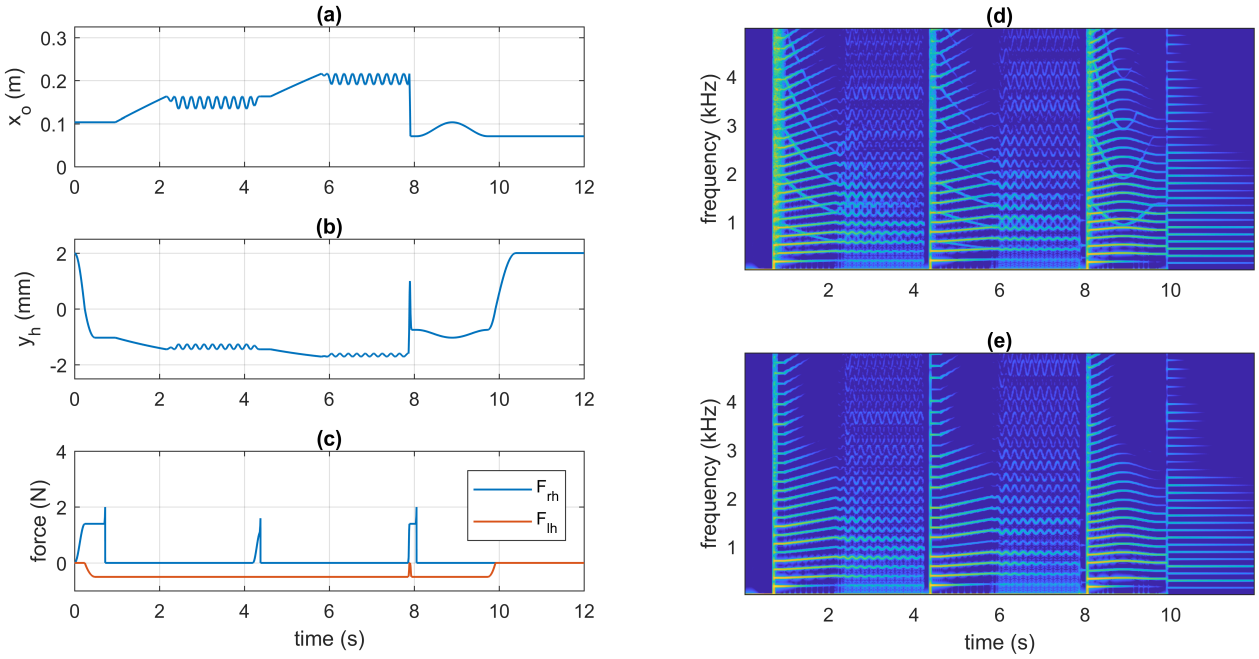

Figure 3: *(a)-(c) Control input signals used for the three-slide phrase; (d)-(e) Spectrogram of the three slides without (d) and with (e) left-hand finger damping.*

where

$$\mathcal{B} = q_o^{n-1} + \mathcal{B}' y_o^n + \mathcal{C}' y_o^{n-1} + \mathcal{D}'^n - \left(\mathbf{g}_o^{(n+1)}\right)^T \Delta_x \mathfrak{L}_o, \tag{69}$$

$$\mathcal{C} = \frac{k_o}{2}\left[E_o' \Delta_x \left(\mathbf{g}_o^{(n+1)}\right)^T \mathbf{g}_o^n - \mathcal{E}'\right]. \tag{70}$$

We know from [19, 16] that (68) has the branched analytical solutions, which are reproduced in the appendix. Once we solve for s_o, we can compute F_o^n using (65). Subsequently, we can use F_o^n in (62) to compute $\mathbf{u}_o^{n+1}$.

4. NUMERICAL SIMULATION

Slide articulatory gestures usually involve a combination of glissando, vibrato, slide attachment, slide detachment and finger damping. To demonstrate the working of the model for these typical slide articulatory actions, a three-slide phrase is simulated by varying the control inputs similar to a player. The simulated control input signals are shown in Figure 3 (a)-(c), and the output spectrograms without and with left-hand finger damping are shown in Figure 3 (d) and (e). These control signals are simulated assuming a constant hand force F_h while the slide is in contact with the string. This is not unreasonable as players generally try to keep F_h approximately constant during sliding.

Before the slide attaches to the string, the right-hand finger force F_{rf} is increased, thereby drawing the string up. Since the right-hand finger damping is varied in proportion to F_{rf} (see equation (11)), this action ensures that the string is damped before the slide attaches to it and the attachment transient is suppressed. This is reflected in the spectrograms as a heavily suppressed region at very low frequency just after the attachment which quickly dies down.

Once the pluck is released (around 800 ms), the first slide comprising of a glissando followed by a vibrato (between the current note and a note that is one semitone downwards in pitch) is articulated. To simulate the glissando, x_o is monotonically increased (the slide is moved closer to the bridge) and to simulate the vibrato it is varied in a sinusoidal fashion. Hand vertical position y_h is varied according to the constant F_h assumption. During the glissando and vibrato, the spectrograms show a low-to-high and a sinusoidal movement in the frequency of the harmonics, respectively, as expected. Of particular interest here is the observation that the high frequency partials (those above 3.5 kHz) which have decayed during the glissando are rejuvenated in the vibrato phase. In addition, the spectrograms show the presence of dense regions, particularly in the frequency range below 1 kHz. These occur because, during the vibrato, the contact position x_o varies at a faster rate (see Figure 3 (a)), which results in more significant driving power contribution from the term $\frac{dx_o}{dt}\frac{\partial u}{\partial x}\Big|_{x=x_o}$ in equation (20). These give a noise-like nature to the synthesised sound during vibrato phases.

Without lifting the slide, a second pluck is released just after 4 s and another similar glissando followed by a vibrato is simulated. Just before 8 s, the right-hand finger is used to push the string up again and within the same period, the slide detaches from the string and re-attaches at a point much closer to the nut. After the re-attachment, a sinusoidal glissando is simulated.

In Figure 3 (d), we see some of the harmonics moving from a higher to a lower frequency, though the slide is simulated to move closer to the bridge. These are the harmonics produced by the non-speaking length due to waves travelling between the nut and the point of slide contact in the absence of left-hand finger damping. Further, the harmonics above 3 kHz are less sustained in Figure 3 (e), showing that there is greater loss of energy with left-hand

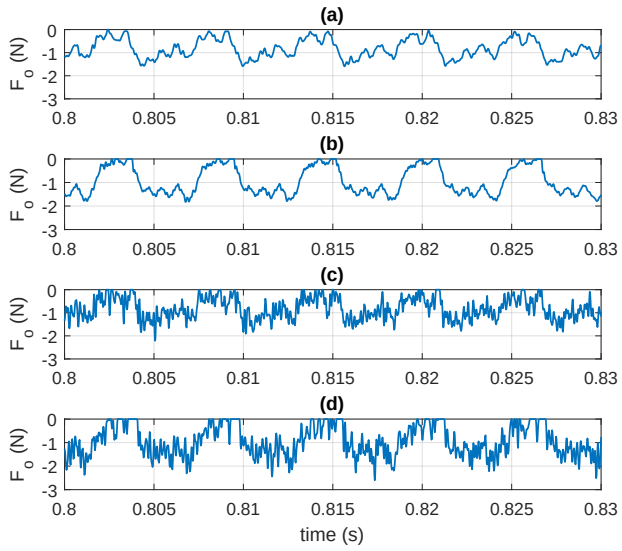

Figure 4: *Influence of left-hand finger damping and hand compliance (k_h and r_h) on the slide-string contact force F_o.*

finger damping.

Observe that while there is no further excitation from the right-hand finger, the detachment of the slide, just before the 10 s mark, causes a detachment transient. This is because the sudden removal of both the slide mass and the left-hand finger extends the vibrations to the non-speaking part of the string, with the pitch dropping to the open string tuned to D3.

A particular feature of interest in the spectrograms is the presence of rattling phases, which can be observed as bright regions spanning all frequencies just after each pluck in Figure 3(d), and just after the first and third pluck in Figure 3 (e) as well, though it is less pronounced in (e) due to left-hand finger damping.

From four simulations (a)-(d), time-domain plots of the contact force F_o are shown in Figure (4) over a 30 ms window shortly after the initial pluck of the simulation, zooming into the rattling phase. In (a) and (b), left-hand damping is enabled, while it is absent ($r_\mathrm{lf} = 0$) in (c) and (d). Further, in (b) and (d) there is no hand compliance ($k_\mathrm{h} = 10^{10}$ and $r_\mathrm{h} = 0$), i.e, the sliding hand is very rigid and undamped. It is clear that, as we move from (a) to (d), rattling is sustained longer, the collisions grow denser, and the high-frequency content increases. The reader can further explore the influence of the finger damping mechanisms and hand compliance on rattling effects aurally via the sound examples listed on the companion website [4].

5. CONCLUDING REMARKS AND PROSPECTS

The presented work is part of the EC Horizon funded VRACE project [5] that seeks to introduce extended parameter time-variance in physics-based simulations of mechano-acoustic vibrating systems. Articulation is one of the key forms of interaction that involves such time variance, with relevance to the wider topic of audio for virtual reality. The project investigates this with a specific focus on the design and development of *virtual-acoustic musical instruments*, which requires that design choices are co-informed by considerations and criteria related to acoustic modelling, numerical methods, sensing, and skilful articulation. The set of strategic design choices listed at the end of Section 1 have been arrived at through this holistic approach, and represents the main methodological novelty of the paper.

The simulation results exemplify various articulatory gestures, including glissandi, vibrato, and slide detachment. They also demonstrate the specific influence of the various damping mechanisms involved in slide articulation, in particular how these co-shape the rattling behaviour. This non-linear feature is intrinsic to slide-string articulation, and the sound examples suggest incorporating these can help evoking a sense of articulatory realism. As such, the results are promising with regard to future real-time implementation of the model in conjunction with developing a bespoke controller.

Perhaps the most interesting observation made in the analysis of the simulation results is that, even though slide-string friction is not explicitly modelled, the output nonetheless can exhibit noise-like components, particularly so during vibrato phases. These components can be directly linked to the articulatory power sources appearing in the system power balance. This finding implies that the notion of *sliding noise*, which so far has been thought of as being a purely friction-based phenomenon (see e.g. [5, 6]), may have to be reconsidered. In other words, the perceived noise-like components in, for example, acoustic slide guitar playing are probably a mix of friction and restoring force-based phenomena, and as such worthy of further investigation.

Further extensions to the proposed model include adding horizontal and longitudinal polarisations, which have been suggested to be of importance to slide-string modelling in [5, 6], and adding tension modulation (for example, following the approach in [20]).

The runtime of the current Matlab implementation is, on an average, approximately 4.5x real-time. It is worthwhile noting that the nodal displacement updates themselves take up only about 13% of the total runtime, but the routines for updating the time-varying parameters and associated vectors and matrices consume about 85% of the total runtime, as shown in Table 1 (input read operations take up the remaining ~2% of runtime). This is largely due to the parameter update routines running at the audio rate in the current implementation. Hence future optimisation strategies are likely to revolve around (i) investigating the optimal control rate at which the parameter updates need to be made, and (ii) how these updates can be performed most efficiently.

Table 1: *Computation times for various updates as percentages of the total simulation runtime*

Update type	Slide subsystem	Left-hand finger subsystem	Right-hand finger subsystem	Non-contact subsystem	Cumulative
Parameter update	19.2%	26.7%	23.8%	15.4%	85.1%
Nodal displacement update	3.6%	3.6%	3.2%	2.8%	13.2%

Finally, to formally study a range of musician's performatory actions during slide articulation, techniques like motion capture could be employed. Integrating such studies with holistic modelling approaches such as the one presented in this paper could feed in to a general methodology to investigate skilful articulation.

[4] Companion website: https://abhiram1989.wixsite.com/slidestringfdmodel
[5] VRACE project website: http://vrace-etn.eu/

6. REFERENCES

[1] S. Bilbao, *Numerical Sound Synthesis: Finite Difference Schemes and Simulation in Musical Acoustics*, Wiley Publishing, 2009.

[2] V. Välimäki, J. Pakarinen, C. Erkut, and M. Karjalainen, "Discrete-time modelling of musical instruments," *Reports on Progress in Physics*, vol. 69, no. 1, pp. 1–78, 2005.

[3] S. Bilbao and A. Torin, "Numerical simulation of string/barrier collisions: The fretboard," in *Proceedings of the 17th International Conference on Digital Audio Effects*, 2014.

[4] G. Evangelista, "Physical model of the string-fret interaction," in *Proceedings of the 14th International Conference on Digital Audio Effects, DAFx 2011*, 2011.

[5] J. Pakarinen, T. Puputti, and V. Välimäki, "Virtual slide guitar," *Computer Music Journal*, vol. 32, no. 3, pp. 42–54, 2008.

[6] G. Evangelista, "Physical model of the slide guitar: An approach based on contact forces," in *Proceedings of Audio Engineering Society Convention 132*, 2012.

[7] J. Pakarinen and T. Puputti, "Slide guitar synthesizer with gestural control," in *Proceedings of the New Interfaces for Musical Expression (NIME) Conference*, 2008.

[8] J. Pakarinen, M. Karjalainen, V. Valimaki, and S. Bilbao, "Energy behavior in time-varying fractional delay filters for physical modeling synthesis of musical instruments," in *Proceedings of the IEEE International Conference on Acoustics, Speech, and Signal Processing (ICASSP '05)*, 2005, vol. 3, pp. iii/1–iii/4.

[9] S. Bilbao, "Time-varying generalizations of all-pass filters," *IEEE Signal Processing Letters*, vol. 12, pp. 376 – 379, 2005.

[10] G. Evangelista and F. Eckerholm, "Player–instrument interaction models for digital waveguide synthesis of guitar: Touch and collisions," *IEEE Transactions on Audio, Speech, and Language Processing*, vol. 18, no. 4, pp. 822–832, 2010.

[11] C. Desvages and S. Bilbao, "Two-polarisation physical model of bowed strings with nonlinear contact and friction forces, and application to gesture-based sound synthesis," *Applied Sciences*, vol. 6, no. 5, pp. 135, 2016.

[12] S. Bilbao, A. Torin, and V. Chatziioannou, "Numerical modeling of collisions in musical instruments," *Acta Acustica united with Acustica*, vol. 101, no. 1, pp. 155–173, 2015.

[13] V. Chatziioannou and M. van Walstijn, "Energy conserving schemes for the simulation of musical instrument contact dynamics," *Journal of Sound and Vibration*, vol. 339, pp. 262–279, 2015.

[14] M. Ducceschi and S. Bilbao, "Non-iterative solvers for nonlinear problems: the case of collisions," in *Proceedings of the 22nd Conference of Digital Audio Effects (DAFx-19)*, Birmingham, UK, September 2019.

[15] S. Willemsen, S. Bilbao, and S. Serafin, "Real-time implementation of an elasto-plastic friction model applied to stiff strings using finite difference schemes," in *Proceedings of the 22nd International Conference on Digital Audio Effects (DAFx-19)*, 2019.

[16] M. van Walstijn, J. Bridges, and S. Mehes, "A real-time synthesis oriented Tanpura model," in *Proceedings of the 19th International Conference on Digital Audio Effects (DAFx-16)*, 2016, pp. 175–182.

[17] F. Gulmammadov, "Analysis, modeling and compensation of bias drift in MEMS inertial sensors," in *4th International Conference on Recent Advances in Space Technologies*, 2009, pp. 591–596.

[18] N. H. Fletcher and T. D. Rossing, *The Physics of Musical Instruments, Second edition*, Springer, 1998.

[19] S. Bilbao, "Numerical modeling of string barrier collisions.," in *Proceedings of the International Symposium on Musical Acoustics (ISMA)*, 2014.

[20] M. Ducceschi and S. Bilbao, "Non-iterative, conservative schemes for geometrically exact nonlinear string vibration," in *Proceedings of the International Conference on Acoustics (ICA 2019)*, Aachen, Germany, September 2019.

7. APPENDIX

The update scalars and matrices in equations (60) - (63) and equation (67) are given in Table 2, where $\mathbf{I}_{\phi}^{n}$ represents the identity matrix of dimensions $|\mathcal{M}_{\phi}^{n}|$ x $|\mathcal{M}_{\phi}^{n}|$, $M_{\mathrm{o}} = \frac{m_{\mathrm{o}}}{\Delta_t^2}$, and $R_{\mathrm{h}} = \frac{r_{\mathrm{h}}}{2\Delta_t}$. Further, denoting $q = q_o^{n-1}$, the branched solutions for (68) can be written as [19, 16]:

Table 2: *Update scalars and matrices.*

Update scalar/ matrix	ϕ	Expression
B_{ϕ}	nc, o	$\frac{2}{\gamma_0+1}$
C_{ϕ}	nc, o	$\frac{\gamma_0-1}{\gamma_0+1}$
$\mathbf{B}'_{\phi}$	nc, o	$\frac{(\lambda^2+\gamma_2)\mathbf{D}_{2,\phi}^{n+1}-\beta^2\mathbf{D}_{4,\phi}^{n+1}}{\gamma_0+1}$
$\mathbf{C}'_{\phi}$	nc, o	$\frac{-\gamma_2\mathbf{D}_{2,\phi}^{n+1}}{\gamma_0+1}$
$\mathbf{A}_{\phi}$	rf, lf	$(\gamma_0+1)\mathbf{I}_{\phi}^{n+1}+\alpha\mathbf{R}_{\phi}^{n}$
B_{ϕ}	rf, lf	2
$\mathbf{C}_{\phi}$	rf, lf	$(\gamma_0-1)\mathbf{I}_{\phi}^{n+1}+\alpha\mathbf{R}_{\phi}^{n}$
$\mathbf{B}'_{\phi}$	rf, lf	$(\lambda^2+\gamma_2)\mathbf{D}_{2,\phi}^{n+1}-\beta^2\mathbf{D}_{4,\phi}^{n+1}$
$\mathbf{C}'_{\phi}$	rf, lf	$-\gamma_2\mathbf{D}_{2,\phi}^{n+1}$
E'_{ϕ}	o	$\frac{\xi}{\gamma_0+1}$
$\mathcal{B}'$		$\frac{2M_{\mathrm{o}}}{R_{\mathrm{h}}+M_{\mathrm{o}}+\frac{k_{\mathrm{h}}}{2}}$
$\mathcal{C}'$		$\frac{R_{\mathrm{h}}-M_{\mathrm{o}}-\frac{k_{\mathrm{h}}}{2}}{R_{\mathrm{h}}+M_{\mathrm{o}}+\frac{k_{\mathrm{h}}}{2}}$
$\mathcal{D}'$		$\frac{\left(\frac{k_{\mathrm{h}}}{2}+R_{\mathrm{h}}\right)y_{\mathrm{h}}^{n+1}+\left(\frac{k_{\mathrm{h}}}{2}-R_{\mathrm{h}}\right)y_{\mathrm{h}}^{n-1}}{R_{\mathrm{h}}+M_{\mathrm{o}}+\frac{k_{\mathrm{h}}}{2}}$
$\mathcal{E}'$		$\frac{-1}{R_{\mathrm{h}}+M_{\mathrm{o}}+\frac{k_{\mathrm{h}}}{2}}$

$$\text{if} \quad q \leq 0 \quad \text{and} \quad q \leq \mathcal{B} : s_{\mathrm{o}} = -\mathcal{B} \tag{71}$$

$$\text{if} \quad q \leq 0 \quad \text{and} \quad q > \mathcal{B} : s_{\mathrm{o}} = \frac{-\mathcal{B} - 2\mathcal{C}q + \sqrt{\mathcal{B}^2 + 4\mathcal{C}q(\mathcal{B}-q)}}{2(1+\mathcal{C})} \tag{72}$$

$$\text{if} \quad q > 0 \quad \text{and} \quad \mathcal{B} \leq q(1-\mathcal{C}) : s_{\mathrm{o}} = -\frac{\mathcal{B}+2\mathcal{C}q}{1+\mathcal{C}} \tag{73}$$

$$\text{if} \quad q > 0 \quad \text{and} \quad \mathcal{B} > q(1-\mathcal{C}) : s_{\mathrm{o}} = -\tfrac{1}{2}\mathcal{B} - \tfrac{1}{2}\sqrt{\mathcal{B}^2 + 4\mathcal{C}q^2} \tag{74}$$